Homolytic B–Cl bond dissociation energies of chloroborane-type molecules

Wen Lu, Robert J. O'Reilly*

Jiangsu Bobujin Biotechnology Co,. Ltd., No. 428, Zhennan Road, High-tech Zone, Gaoxin district, Hai'an, Jiangsu, China, 226600

* Corresponding author: doctororeilly@hotmail.com; ORCID ID: 0000-0002-5000-1920

ABSTRACT

This study reports accurate gas-phase homolytic B–Cl bond dissociation energies, obtained using the benchmark-quality W1w thermochemical protocol, for a set of 25 chloroborane-type molecules (known herein as the BCl25BDE dataset). The BDEs of these species differ by as much as 136.6 kJ mol^{-1} at 298 K, with $(BH_2)_2BCl$ having the lowest BDE (388.5 kJ mol^{-1} at 298 K) and $(CH_3)HBCl$ having the highest (525.1 kJ mol^{-1}). Using the W1w BDEs as reference values, the accuracy of a diverse set of more economical DFT procedures (which may be applied to the study of molecules sufficiently large that the use of benchmark-quality methods such as W1w is rendered computationally prohibitive) have been investigated. As a result of this analysis, the most accurate methods for the computation of B–Cl BDEs are ωB97/A'VQZ (MAD = 3.0 kJ mol^{-1}) and M06/A'VTZ (MAD = 3.2 kJ mol^{-1}). The double-hybrid functional DSD-PBEP86 in conjunction with the A'VQZ basis set (MAD = 4.0 kJ mol^{-1}) was found to give the lowest largest deviation (LD = 6.4 kJ mol^{-1}) of any of methods considered in this assessment study.

Keywords: Chloroborane, bond dissociation, B-Cl bond, homolytic, DFT, W1w theory

INTRODUCTION

Chloroboranes and related derivatives (*i.e.*, R^1R^2B–Cl) are versatile reagents with applications in synthetic organic chemistry and industrial processes. With respect to their use in organic synthesis, chloroborane-type species have been employed in several useful transformations, including hydroboration reactions [1, 2] and the asymmetric reduction of prochiral ketones [3, 4]. Chloroborane-type species have also been used in the synthesis of BN-embedded *p*-quinodimethane derivatives [5], subphthalocyanines [6], new phosphaboretane ring and PB cage compounds [7], and aminoboranes [8], to name but a few. In addition, 2-(dialkylamino)phenylboranes containing the -BXZ group (X, Z = C_6F_5, Cl, and H) have been shown to cleave H_2 under mild conditions [9]. Regarding industrial applications, species such as boron trichloride (BCl_3) have been employed in the etching of thin films composed of various substances, including, for example: GaN [10], TiO_2 [11], Al-doped ZnO [12] and AlN [13].

Given the synthetic and industrial utility of chloroborane-type species, an understanding of their thermochemical properties would be desirable. For example, knowledge of the strength of B–Cl bonds toward homolytic cleavage (*i.e.*, the homolytic bond dissociation energies, BDEs) would be insightful (Scheme 1). However, at present, there appears to be very little reliable data reported in the literature concerning this most fundamental thermochemical property of such species. Indeed, to the best of our knowledge, the only available data regarding the strength of chloroborane-type species toward homolytic B–Cl bond dissociation, is limited to the three species in the series $H_{(3-n)}BCl_n$ [14]. By any measure, this represents a very limited set of molecules, and consequently, a void exists in the literature concerning the effect of a broader range of substituents in affecting the strength of B–Cl bonds toward homolytic cleavage in the gas phase.
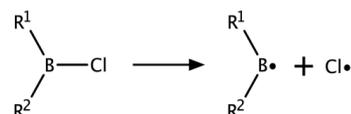
To address this void, the present investigation consists of two parts. First, the highly accurate W1w

thermochemical protocol [15], which represents a layered extrapolation to the all-electron, relativistic CCSD(T) basis-set-limit energy, has been employed to obtain a benchmark-quality dataset of 25 B–Cl BDEs (referred to as the BCl25BDE dataset) with a diverse range of substituents attached to the central boron atom, thus greatly expanding the amount of reliable data pertaining to the gas-phase homolytic dissociation of the B–Cl bonds of chloroborane-type molecules. The W1w protocol has shown robust performance for the calculation of BDEs, achieving, for example, a mean absolute deviation of just 2.1 kJ mol^{-1} when assessed against the BDEs contained within the highly accurate W4-11 dataset [16]. Chan and Radom utilized the W1w protocol for the generation of a comprehensive dataset consisting of 261 BDEs (referred to as the BDE261 dataset) [17], while the W1w protocol has also been employed previously to obtain benchmark-quality datasets for the dissociation of, for example, C–Cl [18] and S–F bonds [19]. Second, we have evaluated the performance of a diverse range of density functional theory (DFT) methods for their ability to compute B–Cl BDEs, using the BCl25BDE dataset as a reference. The best performing method(s) may be used for the computation of accurate homolytic B–Cl BDEs in the case of molecules that are too large to be studied using the W1w protocol.

EXPERIMENTAL

Computational methods: The calculations reported in this study have been performed using the GAMESS program [20]. Geometries of all species were optimized using the B3LYP/A'VTZ level of theory. In a recent assessment study, the B3LYP functional was shown to offer excellent performance for the computation of the geometries of equilibrium species [21]. In particular, it was shown to exhibit a very favorable root-mean-square-deviation (of just 0.0059 Å) when assessed against all bond lengths of the 122 molecules contained in the W4-11-GEOM dataset. In this article, the notation A'VnZ (for n = D, T, and Q) indicates that combination of cc-pVnZ basis sets on H atom, aug-cc-pVnZ basis sets for first row atoms, and aug-cc-pV(n+d)Z basis sets for second row elements [22, 23]. The validity of all structures as being equilibrium in nature (*i.e.*, not transition states) was confirmed by way of harmonic vibrational frequency calculations at the same level of theory, ensuring the absence of any imaginary frequencies.

Benchmark-quality B–Cl BDEs were obtained using the W1w thermochemical protocol. The procedure for performing W1w calculations has been defined in detail in Ref. 15. The zero-point vibrational energy (ZPVE) and enthalpy (H_{vib}(298 K)) corrections resulting from the harmonic vibrational frequency calculations (*i.e.*, those obtained at the B3LYP/A'VTZ level) have been used to correct the relativistic bottom-of-the-well W1w BDEs to values at 0 K (BDE$_0$) and 298 K (BDE$_{298}$).

These corrections have been scaled according to literature scaling factors, namely 0.9884 for the ZPVE and 0.9987 for H_{vib}(298 K) [24]. In addition, an atomic spin-orbit correction of 3.52 kJ mol^{-1} has been included for Cl• [25].

Finally, the performance of a wide range of DFT methods have been assessed against the bottom-of-the-well all-electron, non-relativistic B–Cl BDEs (reported as BDE$_{BM}$ in Table 1, which constitute bottom-of-the-well, all-electron, non-relativistic BDEs without the inclusion of the spin orbit correction for chlorine atom. The DFT functionals that have been employed in this assessment study include: (i) the pure generalizable gradient approximation (GGA) functionals: BP86 [26, 27], BLYP [26, 28], PBE [29, 30], B97-D [31], HCTH407 [32], and N12 [33]; (ii) the meta-GGAs (MGGA): M06-L [34], TPSS [35], τ-HCTH [36], VSXC [37], M11-L [38], and MN12-L [39]; (iii) the hybrid-GGAs (HGGA): BH&HLYP [40], B3LYP [28, 41], B3P86 [27,41], B3PW91 [41, 42], PBE0 [43], B97-1 [44], B98 [45], X3LYP [46], and SOGGA-11X [47]; (iv) the hybrid-meta GGAs (HMGGA): M06 [48], M06-2X [48], BMK [49], TPSSh [35, 50], and τ-HCTHh [36]; (v) the range-separated functionals (RS): CAM-B3LYP [51], LC-ωPBE [52, 53], ωB97 [54], ωB97X [54], ωB97X-D [55], HSE06 [56], N12-SX [57], MN12-SX [57], and M11 [58]; and (vi) the double-hybrid DFTs (DHDFT): B2-PLYP [59], B2-PLYP-D3 [60], B2GP-PLYP [61], B2K-PLYP [62], mPW2-PLYP [63], and DSD-PBEP86 [64]. For selected functionals, we have also included empirical D3 dispersion corrections [60, 65, 66], which make use of the Becke-Johnson damping potential as recommended in Ref. 60 (denoted by the suffix -D3).

RESULTS AND DISCUSSION

Dataset of Homolytic Gas-Phase B–Cl BDEs: The set of 25 gas-phase homolytic B–Cl BDEs, obtained using the benchmark-quality W1w thermochemical protocol (referred here as the BCl25BDE dataset) is presented in Table 1. In addition to the B–Cl BDEs at 0 K and 298 K (denoted as BDE$_0$ and BDE$_{298}$, respectively), an additional set of BDEs, referred to as BDE$_{BM}$, have also been included in Table 1. The BDE$_{BM}$ values constitute bottom-of-the-well all-electron, non-relativistic BDEs, without the inclusion of a spin-orbit correction for chlorine atom, that are used in assessing the performance of DFT methods for their ability to accurately compute B–Cl BDEs (next section). In addition, we have also included the equilibrium B–Cl bond lengths (r_{B-Cl}).

For the species in this set, we note that the B–Cl BDEs (at 298 K) differ by as much as 136.6 kJ mol^{-1}. The monomethyl-substituted molecule, (CH$_3$)HBCl, gives rise to the largest BDE (525.1 kJ mol^{-1}), while (BH$_2$)$_2$BCl has the lowest BDE (388.5 kJ mol^{-1}). Compared with the BDE of the parent molecule, H$_2$BCl (524.6 kJ mol^{-1}), in all but one case (*i.e.*, (CH$_3$)HBCl), introduction of the selected substituents lower the B–Cl BDEs.

Table 1. Homolytic gas-phase bond dissociation energies for a set of 25 chloroborane-type species (obtained using the W1w thermochemical protocol with all energies expressed in kJ mol^{-1}).

R^1	R^2	BDE$_{BM}$	BDE$_0$	BDE$_{298}$	r_{B-Cl} (Å)
BH$_2$	BH$_2$	397.4	385.6	388.5	1.793
AlH$_2$	AlH$_2$	429.1	420.1	421.8	1.795
NH$_2$	BH$_2$	432.5	418.3	422.0	1.809
BH$_2$	F	433.0	419.8	423.6	1.776
BH$_2$	H	441.8	426.6	430.8	1.764
AlH$_2$	H	473.0	459.6	462.7	1.767
PH$_2$	PH$_2$	492.7	480.1	483.5	1.769
Cl	Cl	505.9	493.2	496.9	1.746
HC$_2$	H	514.6	494.5	499.7	1.754
SH	H	513.4	497.5	501.8	1.755
PH$_2$	H	514.1	498.3	502.4	1.754
Cl	F	515.2	501.7	505.7	1.747
SiH$_3$	H	518.8	502.1	506.1	1.749
CN	H	521.2	502.6	507.3	1.733
Cl	H	523.5	506.5	511.2	1.743
OH	OH	522.3	507.8	512.2	1.800
F	F	522.4	508.2	512.5	1.748
NH$_2$	H	531.4	514.2	518.9	1.779
OH	H	532.4	515.0	519.9	1.776
CH$_3$	NH$_2$	531.7	516.1	520.2	1.800
NH$_2$	NH$_2$	532.0	516.1	520.5	1.802
F	H	534.9	516.7	521.8	1.751
CH$_3$	CH$_3$	536.8	520.7	524.5	1.784
H	H	540.7	518.8	524.6	1.742
CH$_3$	H	539.5	520.6	525.1	1.761

Perhaps the most notable effect to emerge from this study concerns the magnitude by which substitution by one or two -BH$_2$ substituents, and to a somewhat smaller extent, -AlH$_2$ group(s), reduce the energies necessary to induce gas-phase homolytic B–Cl bond dissociation. For example, substitution with a single -BH$_2$ substituent (as in (BH$_2$)HBCl) lowers the BDE by 93.8 kJ mol^{-1} compared with that of H$_2$BCl, while substitution with two -BH$_2$ substituents lowers the BDE by 136.1 kJ mol^{-1}. Delocalization effects in the -BH$_2$ substituted product radicals are likely a significant contributor to the significantly lower BDEs of these molecules. The extent of such delocalization effects is revealed by inspection of the spin densities of the product radicals. For example, at the B3LYP/A'VTZ level, the substituent boron atom in (BH$_2$)HB• is associated with a spin density of 0.331, whilst for the (BH$_2$)$_2$B• radical, each substituent boron atom has a spin density of 0.170. Regarding substitution with -AlH$_2$ group(s), the presence of one such substituent (as in (AlH$_2$)HBCl) lowers the B–Cl BDE by 61.9 kJ mol^{-1} compared with that of H$_2$BCl, while the presence of two such substituents (as in (AlH$_2$)$_2$BCl) lower the BDE by 102.8 kJ mol^{-1}. The smaller extent of BDE reduction in species substituted with -AlH$_2$ group(s), compared with those containing -BH$_2$ group(s), may be accounted for, in part, due to a reduced extent of delocalization in the

aluminium-substituted radicals. For example, we find that the spin density on the aluminium atom in (AlH$_2$)HB• (0.174) is significantly lower than the spin density of the boron atom of the -BH$_2$ substituent in (BH$_2$)HB• (0.331). The decreased extent of delocalization of the unpaired electron in the case of radicals containing aluminium-based substituents versus those with -BH$_2$ substituents may arise, in part, because of a relative mismatch in orbital size between the smaller half-filled 2p-orbital on the central boron atom and the larger formally vacant 3p-orbital(s) of the aluminium substituent(s), which would be expected to limit the extent of orbital overlap. Concerning the geometric parameters of chloroborane-type molecules, for a small number of molecules (necessarily limited by the scarcity of previously reported reliable experimental data), it has been possible to compare the theoretically-determined B–Cl bond lengths, as well as several other geometric parameters, with those obtained using experimental methods. Beginning with H$_2$BCl, the computed B–Cl bond length of 1.742 Å is in generally good agreement with the value of 1.735 Å reported by Kawashima *et al.,* which was determined using microwave spectroscopy [67], while good agreement is also noted for the B–H bond lengths (which differ by 0.008 Å) and the H–B–H angles (differing by just 0.4°). Regarding the geometry of dichloroborane (HBCl$_2$), the computed B–Cl bond length differs by only 0.008 Å from the spectroscopically-determined value reported by Matsumura and co-workers [68], while there is also good agreement in the bond angles (differing by just 0.4°). The theoretically-determined B–Cl distance of 1.746 Å in BCl$_3$ differs by just 0.004 Å compared with that obtained by Konaka *et al.,* who employed gas electron diffraction [69]. In addition, we note that our B–Cl bond lengths are in good agreement (~0.001 Å in the case of all three molecules) with those obtained by Grant and Dixon [14], who used the more rigorous CCSD(T)/aug-cc-pVTZ level to obtain the geometries of these three species. Finally, we note that when considering the effect of the selected substituents in governing the magnitude of the length of the B–Cl bonds the set of 25 chloroborane-type molecules, the molecules have B–Cl bond lengths that differ by up to 0.076 Å, with (CN)HBCl having the shortest bond length (1.733 Å) and (NH$_2$)(BH$_2$)BCl having the longest (1.809 Å).

Finally, as the B–Cl BDE$_{BM}$ values will be employed for the purposes of assessing a diverse range of lower-cost conventional and double-hybrid DFT methods (see next section), it is of interest to establish whether the inclusion of post-CCSD(T) corrections, which are not included in the W1w thermochemical protocol, are likely to have a significant effect on the underlying non-relativistic bottom-of-the-well all-electron energies. An accurate and effective way of assessing this is to use an energy-based diagnostic, namely the percentage of the total atomization energy (TAE) accounted for by the (T) component to the TAE (denoted as %TAE$_e$[(T)])),

which has been reported and validated previously [16]. It has been shown that for species with %TAE$_e$[(T)] ≤ 5.0%, post-CCSD(T) contributions are unlikely to exceed 2.1 kJ mol⁻¹. The %TAE$_e$[(T)] values for the species in the BCl25BDE dataset (both the closed-shell precursors and the product radicals) are well below 5% (ranging from 0.6 to 3.1%), indicating that the inclusion of post-CCSD(T) contributions are unlikely to affect the BDEs to any significant extent, and consequently, further validates the benchmark-quality nature of this dataset of B–Cl BDEs for the purposes of assessing the performance of other theoretical methods.

Performance of DFT methods for the computation of Gas-Phase Homolytic B–Cl BDEs: Having obtained a set of accurate benchmark-quality B–Cl BDEs using the W1w thermochemical protocol, attention is now turned to assessing the performance of a diverse range of DFT methods for their ability to provide quantitatively reliable BDEs. In this study, a selection of functionals from each rung of Jacob's ladder (*i.e.*, the GGAs, MGGAs, HGGAs, HMGGAs, RS and DH methods) have been assessed. The results of this analysis are presented in Table 2. For each method, the mean absolute deviation (MAD), mean deviation (MD), largest deviation (LD) and number of outliers (NO, arbitrarily defined as the number of species with a deviation ≥10 kJ mol⁻¹) have been tabulated.

In addition, the effect of basis set size has also been considered by way of having performed calculations using two basis sets, namely A'VTZ and A'VQZ.Before commenting on the performance of each functional within each class, a few general points emerge upon inspection of the data presented in Table 2. Looking at the data overall, it is of interest to note that only a very small number of the chosen DFT methods (namely M06-L, SOGGA11-X, BMK, M06, ωB97 and DSD-PBEP86) offer performance that falls below the threshold of "chemical accuracy", which has been arbitrarily defined as performance ≤ 4.2 kJ mol⁻¹. Furthermore, there appears to be a general tendency for the more highly empirical functionals (*i.e.*, those with dozens of adjustable parameters) to outperform the more lightly empirical methods. This general observation is consistent with previous studies, for example, when a range of such functionals were assessed against the BDE261 dataset [17].

Of the methods investigated in this study, we note that the best performance is achieved by ωB97/A'VQZ (MAD = 3.0 kJ mol⁻¹ and LD = 7.5 kJ mol⁻¹) and M06/A'VTZ (MAD = 3.2 kJ mol⁻¹ and LD = 9.8 kJ mol⁻¹). The double-hybrid functional DSD-PBEP86 also offers reliable performance (in conjunction with the A'VQZ basis set), with an MAD of 4.0 kJ mol⁻¹, and notably, an LD of just 6.4 kJ mol⁻¹ (the lowest LD of any of the methods surveyed in this study). The worst performing methods are BH&HLYP and BLYP, with MADs in conjunction with the A'VQZ basis set of 36.5 and 36.8 kJ mol⁻¹, respectively.

Several other general points emerge from an analysis of this data. First, for the overwhelming majority of the functionals, better performance is obtained in conjunction with the A'VQZ rather than A'VTZ basis set. For the conventional DFTs, the MADs obtained in conjunction with the A'VQZ basis set are lower than those obtained using the A'VTZ basis set by amounts ranging from 0.1–0.6 kJ mol⁻¹, with the notable exceptions of MN12-L, VSXC and M11-L, where the differences reach 1.2, 1.5 and 2.8 kJ mol⁻¹, respectively. For the double hybrid procedures, which are generally known to exhibit considerably slower basis set convergence, use of the A'VQZ rather than A'VTZ basis set results in improvements in MADs by 2.2 (B2PLYP) to 3.8 kJ mol⁻¹ (DSD-PBEP86). Second, the vast majority of functionals tend to systematically underestimate the BDEs (*i.e.*, the MDs adopt negative values). Third, except for BMK and ωB97X, inclusion of a dispersion correction serves to improve the performance of the underlying functional, with performance improvements ranging from 3.6 (in the case of PBE-D3) to 10.2 kJ mol⁻¹ (in the case of BLYP-D3 and BPBE-D3). For ωB97X and BMK, the inclusion of a dispersion correction results in a deterioration in performance by 3.0 and 6.0 kJ mol⁻¹, respectively. Forth, for the majority of the selected functionals (33 out of 56), the calculation of the BDE of $(NH_2)(BH_2)BCl$ appears to be the most troublesome, giving rise to the largest deviations for these methods.

Attention is now given to considering the performance of the functionals within each class (*i.e.*, GGA, MGGA etc…). For the discussion that follows, given that the A'VQZ basis set is expected to afford results near enough to the basis-set-limit for each of the selected functionals, it will be these values that are quoted.

Beginning with the GGA functionals, for which we have considered 12 such methods, the PBE-D3 functional offers the best performance with an MAD of 7.0 kJ mol⁻¹, an LD of 17.6 kJ mol⁻¹ (observed when predicting the B–Cl BDE of $(BH_2)FBCl$), with only four BDEs having deviations from the W1w reference values of ≥10 kJ mol⁻¹. In contrast, BLYP exhibits the worst performance of any of the functionals considered in the present study, with an MAD of 36.8 kJ mol⁻¹. It is of interest to note that the BLYP functional has also shown relatively poor performance for the computation of C–Cl BDEs [70] (MAD = 30.9 kJ mol⁻¹), N–H and N–Cl BDEs (MADs = 23.7 and 25.2 kJ mol⁻¹, respectively) [71] and N–Br BDEs (MAD = 27.1 kJ mol⁻¹) [72]. The LD of BLYP, amounting to 44.8 kJ mol⁻¹ is associated with the computation of the BDE of $(NH_2)(BH_2)BCl$. Where applicable, augmentation of the GGA functionals with a D3 dispersion correction serves to improve their performance. For BLYP and BPBE, the performance of both functionals is improved by 10.2 kJ mol⁻¹, while for BP86 and PBE, the performance enhancements are somewhat smaller, amounting to 7.9 and 3.6 kJ mol⁻¹, respectively.

Table 2. Performance of a range of density functional theory procedures for the computation of homolytic gas-phase B–Cl bond dissociation energies

Class	Functional	A'VTZ				A'VQZ			
		MAD	MSD	LD	NO	MAD	MSD	LD	NO
GGA	BLYP	37.4	-37.4	45.6	25	36.8	-36.8	44.8	25
	B97-D	32.3	-32.3	41.2	25	32.2	-32.2	40.8	25
	HCTH407	30.6	-30.6	40.5	25	30.1	-30.1	40.0	25
	BLYP-D3	27.2	-27.2	33.9	25	26.6	-26.6	33.2	25
	B97-D3	25.9	-25.9	34.3	25	25.7	-25.7	33.9	25
	BPBE	23.4	-23.4	34.0	25	23.3	-23.3	33.8	25
	BP86	17.6	-17.6	28.6	21	17.4	-17.4	28.3	21
	BPBE-D3	13.3	-13.2	23.4	18	13.1	-13.0	23.4	18
	PBE	10.9	-10.7	22.4	14	10.5	-10.3	21.8	13
	N12	10.1	+10.1	20.6	14	9.9	+9.9	20.6	14
	BP86-D3	9.7	-9.4	19.8	11	9.5	-9.2	19.8	11
	PBE-D3	7.3	-6.2	18.0	5	7.0	-5.8	17.6	4
MGGA	TPSS	25.7	-25.7	32.1	25	25.9	-25.9	32.4	25
	τ-HCTH	24.9	-24.9	35.9	25	24.8	-24.8	35.8	25
	TPSS-D3	19.8	-19.8	23.2	25	19.9	-19.9	23.4	25
	VSXC	17.6	-17.6	37.2	20	16.1	-16.1	34.3	18
	M11-L	7.2	-5.7	15.1	6	10.0	-9.6	17.5	13
	MN12-L	7.7	+5.6	16.1	9	6.5	+1.8	12.8	4
	M06-L	4.4	-3.8	13.4	3	4.0	-2.6	12.2	1
HGGA	BH&HLYP	36.9	-36.9	42.0	25	36.5	-36.5	41.7	25
	B3LYP	30.6	-30.6	36.9	25	30.1	-30.1	36.4	25
	X3LYP	28.2	-28.2	34.4	25	27.7	-27.7	33.9	25
	B3PW91	22.2	-22.2	30.2	25	22.1	-22.1	30.0	25
	B3LYP-D3	22.1	-22.1	27.4	25	21.7	-21.7	26.8	25
	PBE0	14.7	-14.7	22.7	22	14.4	-14.4	22.4	22
	B3PW91-D3	13.7	-13.7	20.2	21	13.6	-13.6	20.0	21
	B98	12.9	-12.9	19.3	18	12.5	-12.5	19.0	17
	B3P86	11.5	-11.5	20.3	13	11.4	-11.4	20.2	13
	PBE0-D3	10.5	-10.5	17.8	12	10.3	-10.3	17.5	12
	B97-1	7.8	-7.7	14.8	7	7.5	-7.4	14.4	5
	SOGGA11-X	4.4	-4.1	10.6	2	4.0	-3.6	10.3	1
HMGGA	TPSSh	26.0	-26.0	32.2	25	26.1	-26.1	32.5	25
	BMK-D3	10.5	+10.5	17.9	15	10.0	+10.0	17.3	14
	τ-HCTHh	10.3	-10.3	18.5	13	10.0	-10.0	18.1	13
	M06-2X	8.4	-8.4	12.8	6	8.9	-8.9	13.8	9
	BMK	4.2	+3.5	8.7	0	4.0	+3.0	8.2	0
	M06	3.2	-3.0	9.8	0	3.5	-3.4	10.8	1
RS	CAM-B3LYP	23.7	-23.7	29.4	25	23.3	-23.3	28.9	25
	LC-ωPBE	21.4	-21.4	26.6	25	21.1	-21.1	26.2	25
	CAM-B3LYP-D3	19.6	-19.6	24.6	25	19.2	-19.2	24.1	25
	LC-ωPBE-D3	16.7	-16.7	21.0	25	16.4	-16.4	20.6	25
	HSE06	16.7	-16.7	24.4	25	16.3	-16.3	24.0	24
	M11	11.2	-10.3	18.1	15	10.9	-10.2	18.0	15
	ωB97X-D	9.9	-9.9	13.3	9	9.9	-9.9	13.3	9
	ωB97X	7.2	-7.2	10.9	2	6.9	-6.9	10.5	2
	N12-SX	5.0	+4.3	10.5	1	4.7	+4.0	10.5	1
	ωB97	3.6	-3.4	8.4	0	3.0	-2.7	7.5	0
DH	B2PLYP	17.8	-17.8	20.5	25	15.4	-15.4	18.3	25
	mPW2PLYP	16.4	-16.4	18.7	25	14.2	-14.2	16.7	25
	B2PLYP-D3	13.6	-13.6	15.7	24	11.2	-11.2	13.5	19
	B2GP-PLYP	13.8	-13.8	15.2	25	10.7	-10.7	12.4	15
	B2K-PLYP	11.4	-11.4	12.7	21	8.0	-8.0	9.5	0
	DSD-PBEP86	7.8	-7.8	9.8	0	4.0	-4.0	6.4	0

Regarding the performance of the MGGA functionals, for which we have considered a total of seven such methods, we note that M06-L offers relatively robust performance, with an MAD of 4.0 kJ mol^{-1}. The largest deviation, amounting to 12.2 kJ mol^{-1} is noted in the case of the BDE of $(PH_2)_2BCl$, while the next largest deviation (9.4 kJ mol^{-1}) is observed in the computation of the BDE of (CN)HBCl. For the calculation of the BDE of the parent molecule, H_2BCl, the M06-L functional offers a deviation of just 0.6 kJ mol^{-1} from the W1w

reference value. Moving to the next best performing MGGA functional, namely MN12-L, we compute an MAD of 6.5 kJ mol^{-1}, and note that unlike M06-L, which tends to underestimate BDEs (MD = −2.6 kJ mol^{-1}), MN12-L has a slight tendency to overestimate them (MD = +1.8 kJ mol^{-1}). In addition, compared with M06-L, we note that the MN12-L functional perform more poorly for the calculation of the BDE of H$_2$BCl (with a deviation of +12.2 kJ mol^{-1}). The worst performing MGGA functionals are TPSS and τ-HCTH, with MADs of 25.9 and 24.8 kJ mol^{-1}, respectively. It should be noted that augmentation of the TPSS functional with a dispersion correction serves to reduce the MAD by 5.9 kJ mol^{-1}, whilst also lowering the LD by 9.0 kJ mol^{-1}.

Moving now to a consideration of the performance of the HGGA functionals, the SOGGA11-X functional emerges as the best performer, with an MAD of 4.0 kJ mol^{-1} and an LD of 10.3 kJ mol^{-1} (for the computation of the BDE of (NH$_2$)(BH$_2$)BCl). In fact, with the exception of BH&HLYP and B3LYP-D3 (for which the LDs are noted in the case of (PH$_2$)$_2$BCl and (HC$_2$)HBCl, respectively), for the rest of the selected HGGA functionals, the worst performance is noted in the case of the computation of the BDE of (NH$_2$)(BH$_2$)BCl. The B97-1 functional emerges as the second best of the selected HGGAs, with an MAD of 7.5 kJ mol^{-1}, and gives rise to five species with deviations that are ≥10 kJ mol^{-1}, compared with only one in the case of SOGGA11-X. The worst performance is noted in the case of BH&HLYP, with an MAD of 36.5 kJ mol^{-1}, no species with deviations from the W1w reference values of less than 10 kJ mol^{-1}, and an LD of 41.7 kJ mol^{-1}. This poor performance is consistent with previous literature reports concerning the use of BH&HLYP for the computation of C–Cl [70], N–H and N–Cl [71], N–Br [72], and S–F BDEs [19]. The immensely popular B3LYP functional also offers relatively poor performance, with an MAD of 30.1 kJ mol^{-1} and an LD of 36.4 kJ mol^{-1}, and as such would not be recommended as a method of choice for the computation of accurate B–Cl BDEs. Regarding inclusion of a D3 correction, which we have probed in the context of three functionals, performance improvements of 4.1, 8.4 and 8.5 kJ mol^{-1} are noted in the case of the PBE0-D3, B3LYP-D3 and B3PW91-D3 functionals, respectively.

Regarding the performance of the HMGGA functionals, we note that both M06 and BMK offer robust performance, with MADs of 3.5 and 4.0 kJ mol^{-1}, respectively. It is of interest to note that although M06 is associated with a slightly lower MAD than BMK (by 0.5 kJ mol^{-1}), the LD of M06 (10.8 mol^{-1}) is larger than that of BMK (8.2 kJ mol^{-1}). Furthermore, although M06 tends to underestimate the BDEs (MD = −3.4 kJ mol^{-1}), the BMK functional tends to overestimate them (MD = +3.0 kJ mol^{-1}). For the parent molecule, H$_2$BCl, M06 performs significantly better than BMK, with a deviation of 0.8 kJ mol^{-1} versus 8.1 kJ mol^{-1} from the W1w reference value. The worst performing HMGGA, by far, is TPSSh

(MAD = 26.1 kJ mol^{-1} and LD = 32.5 kJ mol^{-1}). Finally, we note that augmentation of the BMK functional with a D3 correction serves to decrease the performance, raising the MAD by 6.0 kJ mol^{-1} compared with that of the parent BMK functional. In this context, in the present study, BMK was one of only two functionals (the other being the range-separated functional ωB97X-D) where inclusion of such a correction resulted in a deterioration in performance compared with the non-corrected functional.

Of the range-separated (RS) functionals, the best performing method appears to be ωB97, with an MAD of 3.0 kJ mol^{-1} and an LD = 7.5 kJ mol^{-1} (noted in the case of the computation of the BDE of (NH$_2$)(BH$_2$)BCl), and exhibits a tendency to underestimate the BDEs (MD = −2.7 kJ mol^{-1}). The next best performing method, N12-SX, is associated with an MAD of 4.7 kJ mol^{-1}, and unlike ωB97, tends to overestimate the BDEs (MD = +4.0 kJ mol^{-1}). The LD for N12-SX, amounting to 10.5 kJ mol^{-1}, was noted in the case of the computation of the BDE of H$_2$BCl. Both CAM-B3LYP and LC-ωBPBE offered the worst performance of the considered RS functionals, with MADs of 23.3 and 21.1 kJ mol^{-1}, respectively. The performance of these two functionals was improved slightly upon the inclusion of the D3 correction, with CAM-B3LYP-D3 and LC-ωBPBE-D3 having MADs of 19.2 and 16.4 kJ mol^{-1}, respectively. Regarding the performance of M11, we note that this functional performed significantly worse (MAD = 10.9 kJ mol^{-1}) than that of the HMGGA functional M06 (MAD = 3.5 kJ mol^{-1}).

Finally, we examine the performance of the six selected double-hybrid DFT methods. As mentioned previously, these functionals were found to be somewhat more sensitive to the nature of the basis set compared with the "conventional DFTs", with the difference between the A'VTZ and A'VQZ results amounting to between 2.2 (mPW2PLYP) and 3.8 (DSD-PBEP86) kJ mol^{-1}. Furthermore, all the double-hybrid functionals systematically underestimated the BDEs (*i.e.*, MD = −MAD). The DSD-PBEP86 functional in conjunction with the A'VQZ basis set emerged as the best performing method with an MAD of 4.0 kJ mol^{-1} and an LD of 6.4 kJ mol^{-1} (noted in the case of the computation of the BDE of F$_2$BCl). The LD for DSD-PBEP86 was in fact found to be the lowest of any of the methods investigated in this assessment study. The B2K-PLYP functional, which was optimized for the computation of barrier heights, offered an MAD (8.0 kJ mol^{-1}) that is double that of DSD-PBEP86, and had an LD of 9.5 kJ mol^{-1} (also for the computation of the BDE of F$_2$BCl). The remaining four functionals have MADs that range from 10.7 (B2GP-PLYP) to 15.4 (B2PLYP) kJ mol^{-1}. For these four functionals, the LDs (ranging from 12.4 to 18.3 kJ mol^{-1}) were associated with the calculation of the BDE of (NH$_2$)(BH$_2$)BCl. Finally, we note that the inclusion of a D3 correction served to improve the performance of the B2PLYP functional by 4.2 kJ mol^{-1}.

CONCLUSIONS

In this study, the highly accurate W1w thermochemical protocol (which represents a layered-extrapolation to the all-electron, relativistic, CCSD(T)/CBS limit) has been employed to obtain a benchmark dataset of 25 gas-phase homolytic B–Cl BDEs (referred to herein as the BCl25BDE dataset) of a diverse range of chloroborane-type molecules. The BDEs (at 298 K) range from 388.5 kJ mol^{-1} (in the case of $(BH_2)_2BCl$) to 525.1 kJ mol^{-1} (in the case of $(CH_3)HBCl$). This dataset of BDEs fills a void that currently exists in the literature concerning the strength of B–Cl bonds toward homolytic cleavage, for which at present, only a very limited amount of reliable data currently exists. Having obtained an accurate and chemically diverse dataset, an assessment of more computationally economical conventional and double-hybrid DFT methods has been performed, with the effect of basis set size also examined in the context of both the smaller A'VTZ and larger A'VQZ basis sets. The effect of basis set size on the performance of the conventional DFTs was shown to be modest (typically ranging between 0.1–0.6 kJ mol^{-1}), although was somewhat larger for the double-hybrid DFTs (with differences ranging from 2.2 to 3.8 kJ mol^{-1}). Of the functionals investigated, we find that the best performing methods for the computation of gas-phase homolytic B–Cl BDEs are ωB97/A'VQZ (MAD = 3.0 kJ mol^{-1}) and M06/A'VTZ (MAD = 3.2 kJ mol^{-1}). The double-hybrid functional DSD-PBEP86 also offered reliable performance (with an MAD of 4.0 kJ mol^{-1} when used in conjunction with the A'VQZ basis set) and was associated with the lowest LD (6.4 kJ mol^{-1}) of any of the methods considered in this assessment study.

REFERENCES

1. Altiti A.S., Cheng K.F., He M., Al-Abed Y. (2017) β-Hydroxy-tetrahydroquinolines from quinolines using chloroborane: Synthesis of the peptidomimetic FISLE-412. *Chem. Eur. J.,* **23**, 10738-10743. https://doi.org/ 10.1002/chem.201701944

2. Kanth J.V.B., Brown H.C. (2001) Hydroboration. 97. Synthesis of new exceptional chloroborane−Lewis base adducts for hydroboration. Dioxane−monochloroborane as a superior reagent for the selective hydroboration of terminal alkenes. *J. Org. Chem.,* **66**, 5359-5365. https://doi.org/10.1021/jo015527o

3. Zhang P. (2007) (-)-Diisopinocampheyl chloroborane [(-)-DIP-Chloride™]: A versatile reagent in asymmetric synthesis. *Synlett.*, **17**, 2762-2763. https://doi.org/10.1055/s-2007-991074

4. Chandrasekharan J., Ramachandran P.V., Brown H.C. (1985) Diisopinocampheylchloroborane, a remarkably efficient chiral reducing agent for aromatic prochiral ketones. *J. Org. Chem.,* **50**, 5446-5448. https://doi.org/10.1021/jo00225a109

5. Noguchi M., Suzuki K., Kobayashi J., Yurino T.,

Tsuruji H., *et al*. (2018) Planar and bent BN-embedded *p*-quinodimethanes synthesized by transmetalation of bis(trimethylsilyl)-1,4-dihydropyrazines with chloroborane. *Organometallics*, **37**, 1833-1836. https://doi.org/10.1021/acs.organomet.8b00294

6. Giribabu L., Kumar C.V., Surendar A., Reddy V.B., Chandrasekharam M., *et al.* (2007) Highly efficient microwave-assisted synthesis of subphthalocyanines. *Synth. Commun.* **37**, 4141-4147. https://doi.org/10.1080/00397910701574775

7. Paine R.T., Dou D., Westerhausen M., Duesler E.N., Linti G., Nöth H. (2006) Synthesis and reactivity of borylphosphanes. *Phosphorus Sulfur Silicon Relat. Elem.*, **77**, 61-64. https://doi.org/10.1080/10426509308045619

8. Niedenzu K., Dawson J.W. (1959) Boron-nitrogen compounds II. Aminoboranes, Part 1: The preparation of organic substituted aminoboranes through a grignard reaction. *J. Am. Chem. Soc.*, **81**, 5553-5555. https://doi.org/10.1021/ja01530a010

9. Chernichenko K., Kotai B., Nieger M., Heikkinen S., Papai I., Repo T. (2017) Replacing C_6F_5 groups with Cl and H atoms in frustrated Lewis pairs: H_2 additions and catalytic hydrogenations. *Dalton Trans.,* **46**, 2263-2269. https://doi.org/10.1039/C6DT04649E

10. Lin M.E., Fan Z.F., Ma Z., Allen L.H., Morkoç, H. (1994) Reactive ion etching of GaN using BCl_3. *Appl. Phys. Lett.,* **64**, 887. https://doi.org/10.1063/1.110985

11. Lemaire P.C., Parsons G.N. (2017) Thermal selective vapor etching of TiO_2: Chemical vapor etching via WF_6 and self-limiting atomic layer etching using WF_6 and BCl_3. *Chem. Mater.,* **29**, 6653-6665. https://doi.org/10.1021/acs.chemmater.7b00985

12. Joo Y.-H., Jin M.-J., Kim. S.K., Um D.-S., Kim C.-I. (2021) BCl_3/Ar plasma etching for the performance enhancement of Al-doped ZnO thin films. *Appl. Surf. Sci.,* **561**, 149957. https://doi.org/10.1016/j.apsusc.2021.149957

13. Khan F.A., Zhou L., Kumar V., Adesida I., Okojie R. (2002) High rate etching of AlN using BCl_3/Cl_2/Ar inductively coupled plasma. *Materials Science and Engineering: B*, **95**, 51-54. https://doi.org/10.1016/S0921-5107(02)00160-5

14. Grant D.J., Dixon D.A. (2009) Heats of formation and bond energies of the $H_{(3-n)}BX_n$ compounds for (X = F, Cl, Br, I, NH_2, OH, and SH). *J. Phys. Chem. A*, **113**, 777-787. https://doi.org/10.1021/jp806627r

15. Karton A., Rabinovich E., Martin J.M.L., Ruscic B. (2006) W4 theory for computational thermochemistry: In pursuit of confident sub-kJ/mol predictions. *J. Chem. Phys.,* **125**, 144108(1-16). https://doi.org/10.1063/1.2348881

16. Karton A., Daon S., Martin J.M.L. (2011) W4-11: A high-confidence benchmark dataset for computational thermochemistry derived from first-principles W4 data. *Chem. Phys. Lett.,* **510**, 165-178. https://doi.org/10.1016/j.cplett.2011.05.007

17. Chan B., Radom L. (2012) BDE261: A Comprehensive set of high-level theoretical bond dissociation enthalpies. *J. Phys. Chem. A,* **116**, 4975-4986. https://doi.org/10.1021/jp302542z

18. Garifullina A., Mahboob A., O'Reilly R.J. (2016) A dataset of homolytic C–Cl bond dissociation energies obtained by means of W1w theory. *Chem. Data Collect.,* **3-4**, 21-25. https://doi.org/10.1016/j.cdc.2016.07.003

19. O'Reilly R.J., Balanay M.P. (2019) A quantum chemical study of the effect of substituents in governing the strength of the S–F bonds of sulfenyl-type fluorides toward homolytic dissociation and fluorine atom transfer. *Chem. Data Collect.,* **20**, 100186. https://doi.org/10.1016/j.cdc.2019.100186

20. Schmidt M.W., Baldridge K.K., Boatz J.A., Elbert S.T., Gordon M.S., *et al.* (1993) General atomic and molecular electronic structure system. *J. Comput. Chem.,* **14**, 1347-1363. https://doi.org/10.1002/jcc.540141112

21. Karton A., Spackman P.R. (2021) Evaluation of density functional theory for a large and diverse set of organic and inorganic equilibrium structures. *J. Comput. Chem.,* **42**, 1590. https://doi.org/10.1002/jcc.26698

22. Dunning T.H., Jr. (1989) Gaussian basis sets for use in correlated molecular calculations. I. The atoms boron through neon and hydrogen. *J. Chem. Phys.,* **90**, 1007. https://doi.org/10.1063/1.456153

23. Wilson A.K., Woon D.E., Peterson K.A., Dunning T.H.Jr. (1999) Gaussian basis sets for use in correlated molecular calculations. IX. The atoms gallium through krypton. *J. Chem. Phys.,* **110**, 7667. https://doi.org/10.1063/1.478678

24. Merrick J.P., Moran D., Radom L. (2007) An evaluation of harmonic vibrational frequency scale factors, *J. Phys. Chem. A,* **111**, 11683-11700. https://doi.org/10.1021/jp073974n

25. Curtiss L.A., McGrath M.P., Blaudeau J.-P., Davis N.E., Binning R., Radom L. (1995) Extension of Gaussian-2 theory to molecules containing third-row atoms Ga–Kr. *J. Chem. Phys.,* **103**, 6104-6113. https://doi.org/10.1063/1.470438

26. Becke A. D. (1988) Density-functional exchange-energy approximation with correct asymptotic-behavior. *Phys. Rev. A,* **38**, 3098-3100. https://doi.org/10.1103/PhysRevA.38.3098

27. Perdew J.P. (1986) Density-functional approximation for the correlation energy of the inhomogeneous electron gas. *Phys. Rev. B,* **33**, 8822-8824. https://doi.org/10.1103/PhysRevB.33.8822

28. Lee C., Yang W., Parr R.G. (1988) Development of the Colle-Salvetti correlation-energy formula into a functional of the electron density. *Phys. Rev. B,* **37**, 785-789. https://doi.org/10.1103/PhysRevB.37.785

29. Perdew J.P., Burke K., Ernzerhof M. (1996) Generalized gradient approximation made simple. *Phys. Rev. Lett.,* **77**, 3865-3868. https://doi.org/10.1103/PhysRevLett.77.3865

30. Perdew J.P., Burke K., Ernzerhof M. (1997) Errata: Generalized gradient approximation made simple. *Phys. Rev. Lett.,* **78**, 1396. https://doi.org/10.1103/PhysRevLett.78.1396

31. Grimme S. (2006) Semiempirical GGA-type density functional constructed with a long-range dispersion correction. *J. Comp. Chem.,* **27**, 1787-1799. https://doi.org/10.1002/jcc.20495

32. Boese A.D., Handy N.C. (2001) A new parametrization of exchange-correlation generalized gradient approximation functionals. *J. Chem. Phys.,* **114**, 5497. https://doi.org/10.1063/1.1347371

33. Peverati R., Truhlar D.G. (2012) Exchange-correlation functional with good accuracy for both structural and energetic properties while depending only on the density and its gradient. *J. Chem. Theory Comput.,* **8**, 2310-2319. https://doi.org/10.1021/ct3002656

34. Zhao Y., Truhlar D.G. (2006) A new local density functional for main-group thermochemistry, transition metal bonding, thermochemical kinetics, and noncovalent interactions. *J. Chem. Phys.* **125**, 194101(1-18). https://doi.org/10.1063/1.2370993

35. Tao J.M., Perdew J.P., Staroverov V.N., Scuseria G.E. (2003) Climbing the density functional ladder: Nonempirical meta-generalized gradient approximation designed for molecules and solids. *Phys. Rev. Lett.,* **91**, 146401. https://doi.org/10.1103/PhysRevLett.91.146401

36. Boese A.D., Handy N.C. (2002) New exchange-correlation density functionals: The role of the kinetic-energy density. *J. Chem. Phys.,* **116**, 9559-9569. https://doi.org/10.1063/1.1476309

37. Van Voorhis T., Scuseria G.E. (1998) A novel form for the exchange-correlation energy functional. *J. Chem. Phys.,* **109**, 400-410. https://doi.org/10.1063/1.476577

38. Peverati R., Truhlar D.G. (2012) M11-L: A Local density functional that provides improved accuracy for electronic structure calculations in Chemistry and Physics. *J. Phys. Chem. Lett.,* **3**, 117-124. https://doi.org/10.1021/jz201525m

39. Peverati R., Truhlar D.G. (2012) An improved and broadly accurate local approximation to the exchange-correlation density functional: The MN12-L functional for electronic structure calculations in chemistry and physics. *Phys. Chem. Chem. Phys.,* **10**, 13171. https://doi.

org/10.1039/C2CP42025B

40. Becke A.D. (1993) A new mixing of Hartree–Fock and local density functional theories. *J. Chem. Phys.,* **98**, 1372. https://doi.org/10.1063/1.464304

41. Becke A.D. (1993) Density functional thermochemistry. III. The role of exact exchange. *J. Chem. Phys.,* **98**, 5648. https://doi.org/10.1063/1.464913

42. Perdew J.P., Chevary J.A., Vosko, S.H., Jackson K.A., Pederson M.R., *et al.* (1992) Atoms, molecules, solids, and surfaces: applications of the generalized gradient approximation for exchange and correlation. *Phys. Rev. B,* **46**, 6671. https://doi.org/10.1103/physrevb.46.6671

43. Adamo C., Barone V. (1999) Toward reliable density functional methods without adjustable parameters: The PBE0 model. *J. Chem. Phys.,* **110**, 6158-6169. https://doi.org/10.1063/1.478522

44. Hamprecht F. A., Cohen A., Tozer D.J., Handy N.C. (1998) Development and assessment of new exchange-correlation functionals. *J. Chem. Phys.,* **109**, 6264-6271. https://doi.org/10.1063/1.477267

45. Schmider H.L., Becke A.D. (1998) Optimized density functionals from the extended G2 test set. *J. Chem. Phys.,* **108**, 9624-9631. https://doi.org/10.1063/1.476438

46. Xu X., Goddard W.A.III, (2004) The X3LYP extended density functional for accurate descriptions of nonbond interactions, spin states, and thermochemical properties. *Proc. Natl. Acad. Sci. USA*, **101**, 2673-2677. https://doi.org/10.1073/pnas.0308730100

47. Peverati R., Truhlar D.G. (2011) A global hybrid generalized gradient approximation to the exchange-correlation functional that satisfies the second-order density-gradient constraint and has broad applicability in chemistry. *J. Chem. Phys.,* **135**, 191102. https://doi.org/10.1063/1.3663871

48. Zhao Y., Truhlar D.G. (2008) The M06 suite of density functionals for main group thermochemistry, thermochemical kinetics, noncovalent interactions, excited states, and transition elements: two new functionals and systematic testing of four M06-class functionals and 12 other functionals. *Theor. Chem. Acc.,* **120**, 215-241. https://doi.org/10.1007/s00214-007-0310-x

49. Boese A.D., Martin J.M.L. (2004) Development of density functionals for thermochemical knetics. *J. Chem. Phys.,* **121**, 3405-3416. https://doi.org/10.1063/1.1774975

50. Staroverov V.N., Scuseria G.E., Tao J., Perdew J.P. (2003) Comparative assessment of a new nonempirical density functional: Molecules and hydrogen-bonded complexes. *J. Chem. Phys.,* **119**, 12129. https://doi.org/10.1063/1.1626543

51. Yanai T., Tew D., Handy N. (2004) A new hybrid exchange-correlation functional using the Coulomb-attenuating method (CAM-B3LYP). *Chem. Phys. Lett.,* **393**, 51-57. https://doi.org/10.1016/j.cplett.2004.06.011

52. Vydrov O.A., Scuseria G.E. (2006) Assessment of a long range corrected hybrid functional. *J. Chem. Phys.,* **125**, 234109. https://doi.org/10.1063/1.2409292

53. Vydrov O.A., Heyd J., Krukau A., Scuseria G.E. (2006) Importance of short-range versus long-range Hartree-Fock exchange for the performance of hybrid density functionals. *J. Chem. Phys.* **125**, 074106. https://doi.org/10.1080/00268970500417846

54. Chai J.-D., Head-Gordon M. (2008) Systematic optimization of long-range corrected hybrid density functionals. *J. Chem. Phys.* **128**, 084106 https://doi.org/10.1063/1.2834918

55. Chai J.-D., Head-Gordon M. (2008) Long-range corrected hybrid density functionals with damped atom-atom dispersion corrections. *Phys. Chem. Chem. Phys.,* **10,** 6615-6620. https://doi.org/10.1039/B810189B

56. Heyd J., Scuseria G.E., Ernzerhof M. (2003) Hybrid functionals based on a screened Coulomb potential. *J. Chem. Phys.,* **118**, 8207. https://doi.org/10.1063/1.1564060

57. Peverati R., Truhlar D.G. (2012) Screened-exchange density functionals with broad accuracy for chemistry and solidstate physics. *Phys. Chem. Chem. Phys.,* **14**, 16187. https://doi.org/10.1039/C2CP42576A

58. Peverati R., Truhlar D.G. (2011) Improving the accuracy of hybrid meta-gga density functionals by range separation. *J. Phys. Chem. Lett.,* **2**, 2810-2817. https://doi.org/10.1021/jz201170d

59. Grimme S. (2006) Semiempirical hybrid density functional with perturbative second-order correlation. *J. Chem. Phys.,* **124**, 034108. https://doi.org/10.1063/1.2148954

60. Grimme S., Ehrlich S., Goerigk L. (2011) Effect of the damping function in dispersion corrected density functional theory. *J. Comp. Chem*., **32**, 1456-1465. https://doi.org/10.1002/jcc.21759

61. Karton A., Tarnopolsky A., Lamere J.-F., Schatz G.C., Martin J.M.L. (2008) Highly accurate first-principles benchmark data sets for the parametrization and validation of density functional and other approximate methods. derivation of a robust, generally applicable, double-hybrid functional for thermochemistry and thermochemical kinetics. *J. Phys. Chem. A,* **112**, 12868. https://doi.org/10.1021/jp801805p

62. Tarnopolsky A., Karton A., Sertchook R., Vuzman D., Martin J.M.L. (2008) Double-hybrid functionals for thermochemical kinetics. *J. Phys. Chem. A,*

112, 3. https://doi.org/10.1021/jp710179r

63. Schwabe T., Grimme S. (2006) Towards chemical accuracy for the thermodynamics of large molecules: new hybrid density functionals including non-local correlation effects. *Phys. Chem. Chem. Phys.,* **8**, 4398. https://doi.org/10.1039/B608478H

64. Kozuch S., Martin J.M.L. (2011) DSD-PBEP86: in search of the best double-hybrid DFT with spin-component scaled MP2 and dispersion corrections. *Phys. Chem. Chem. Phys.,* **13**, 20104-20107. https://doi.org/10.1039/C1CP22592H

65. Grimme S., Antony J., Ehrlich S., Krieg H. (2010) A consistent and accurate ab initio parametrization of density functional dispersion correction (DFT-D) for the 94 elements H-Pu. *J. Chem. Phys.,* **132**, 154104. https://doi.org/10.1063/1.3382344

66. Grimme S. (2011) Density functional theory with London dispersion corrections. *WIREs Comput. Mol. Sci.,* **1**, 211. https://doi.org/10.1002/wcms.30

67. Kawashima Y., Takeo H., Sugie M., Matsumura C., Hirota E. (1993) Microwave spectrum of chloroborane, BH$_2$Cl. *J. Chem. Phys.,* **99**, 820. https://doi.org/10.1063/1.465345

68. Sugie M., Takeo H., Matsumura C. (1994) Microwave spectrum of dichloroborane (BHCl$_2$). *Spectrochim. Acta A Mol. Biomol. Spectrosc.,* **50**, 1379-1387. https://doi.org/10.1016/0584-8539(94)E0048-F

69. Shigehiro, K., Yoshitada, M., Kozo, K., Yonezo, M. (1966) The molecular structure and force constants of boron trifluoride and boron trichloride. *Bull. Chem. Soc. Jpn.*, **39**, 1134-1146. https://doi.org/10.1246/bcsj.39.1134

70. Kaliyeva L., Zhumagali S., Akhmetova N., Karton A., O'Reilly R.J. (2016) Stability of the chlorinated derivatives of the DNA/RNA nucleobases, purine and pyrimidine toward radical formation via homolytic C–Cl bond dissociation. *Int. J. Quantum Chem.,* **117**, e25319. https://doi.org/10.1002/qua.25319

71. O'Reilly R.J., Karton A., Radom L. (2011) N–H and N–Cl homolytic bond dissociation energies and radical stabilization energies: An assessment of theoretical procedures through comparison with benchmark-quality W2w data. *Int. J. Quantum Chem.,* **112**, 1862-1878. https://doi.org/10.1002/qua.23210

72. O'Reilly R.J., Karton A. (2016) A dataset of highly accurate homolytic N–Br bond dissociation energies obtained by Means of W2 theory. *Int J. Quantum Chem.,* **116**, 52-60. https://doi.org/10.1002/qua.25024